Toward a hydrodynamic theory of sonoluminescence

Ritva Löfstedt, Bradley P. Barber and Seth J. Putterman

Citation: Physics of Fluids A: Fluid Dynamics **5**, 2911 (1993); doi: 10.1063/1.858700
View online: https://doi.org/10.1063/1.858700
View Table of Contents: https://aip.scitation.org/toc/pfa/5/11
Published by the American Institute of Physics

Toward a hydrodynamic theory of sonoluminescence

Ritva Löfstedt, Bradley P. Barber, and Seth J. Putterman
Department of Physics, University of California, Los Angeles, California 90024

(Received 30 November 1992; accepted 30 June 1993)

For small Mach numbers the Rayleigh–Plesset equations (modified to include acoustic radiation damping) provide the hydrodynamic description of a bubble's breathing motion. Measurements are presented for the bubble radius as a function of time. They indicate that in the presence of sonoluminescence the ratio of maximum to minimum bubble radius is about 100. Scaling laws for the maximum bubble radius and the temperature and duration of the collapse are derived in this limit. Inclusion of mass diffusion enables one to calculate the ambient radius. For audible sound fields these equations yield picosecond hot spots, such as are observed experimentally. However, the analysis indicates that a detailed description of sonoluminescence requires the use of parameters for which the resulting motion reaches large Mach numbers. Therefore the next step toward explaining sonoluminescence will require the extension of bubble dynamics to include nonlinear effects such as shock waves.

I. INTRODUCTION

The passage of a sound wave through a fluid can lead to a spontaneous concentration of energy so spectacular that flashes of light are emitted. Since the imposed sound fields have a Mach number, M, of order 10^{-5} ($M=v/c$, where v is the velocity amplitude of the fluid motion and c is the speed of sound), which corresponds to an energy density of 10^{-11} eV per molecule of fluid, and the emitted photons have energies measured in eV, the focusing factor spans 12 orders of magnitude.[1] In recent experiments the light emission (sonoluminescence or SL) has been controlled, so as to be generated from a single bubble trapped at the velocity node of the sound field (stable SL).[2] These experiments have found that the light consists of flashes, repeating synchronously with the frequency of the imposed audible/ultrasonic sound field, which are less than 50 psec in duration and have a broadband spectrum peaked far into the ultraviolet.[3]

If one could understand theoretically this conversion of sound to light and the characteristics of the light pulses, then perhaps one could predict other experimental arrangements characterized by even greater degrees of energy concentration than those reported in these most recent (yet first) set of measurements of synchronous SL. Also if one could understand the mechanism of SL, then perhaps even shorter flash widths could be designed. Our goal is to set out in this direction by constructing a set of scaling laws that connect SL with the low Mach number solutions to the hydrodynamics of bubble motion. Comparison of the scaling laws with experiment indicates that these laws provide a simple qualitative picture of SL. However, a critical comparison requires that the underlying model be pushed to a regime, where the need for a more sophisticated nonlinear analysis of the Navier–Stokes equations is clear. In the end, a complete picture of SL will even transcend the Navier–Stokes hydrodynamics, which does not include a mechanism for light emission.

The basic description of the motion of a gas-filled bubble in a fluid is the Rayleigh–Plesset equation[4] (derived in the Introduction),

$$R\ddot{R}+\frac{3}{2}\dot{R}^2=\frac{1}{\rho}\left(P_g(R)-P_0+P_a(t)+\frac{R}{c}\frac{d}{dt}\left[P_g(R)+P_a(t)\right]\right), \tag{1}$$

where $R(t)$ is the radius of the bubble, P_0 is the ambient atmospheric pressure, $P_a(t)$ is the acoustic drive at the bubble, $P_g(R)$ is the pressure of the gas inside the bubble, ρ is the fluid density, and c is the speed of sound in the fluid. This equation, where the unimportant contributions of surface tension and viscosity have been neglected, constitutes the force law for the bubble radius: the acceleration of the bubble wall is due to the difference between internal and external pressures. The last term in (1) represents the damping due to the radiation of sound into the fluid by the bubble's motion.[4] The gas pressure is determined by an adiabatic equation of state, including the effect of the van der Waals hard core "a":[5]

$$P_g(R)=\frac{P_0R_0^{3\gamma}}{(R^3-a^3)^{\gamma}},\quad T_g(R)=\frac{T_0R_0^{3(\gamma-1)}}{(R^3-a^3)^{\gamma-1}}. \tag{2}$$

Here R_0 is the ambient radius corresponding to the size at which the bubble contents are at $P_0(=1$ atm) and $T_0(=300$ K), and γ is the ratio of specific heats c_P/c_V.

The richness of the nonlinear R–P equation is apparent from the broad range of time scales characterizing the bubble's motion for typical experimental drive parameters. Typical solutions to the R–P equation are indicated by the solid lines in Figs. 1–3. As shown by Fig. 1, the bubble expands in response to the rarefaction phase of the sound field on a time scale determined by the drive frequency. As the external pressure becomes positive the bubble collapses. This collapse is arrested only by the pressures built up as the bubble's size approaches the excluded volume of the gas inside it, i.e., the hard core. These pressures, and accompanying high temperatures, last for pico- or nanoseconds, as shown in Fig. 3, which is a detailed blowup of

 0899-8213/93/5(11)/2911/18/$6.00

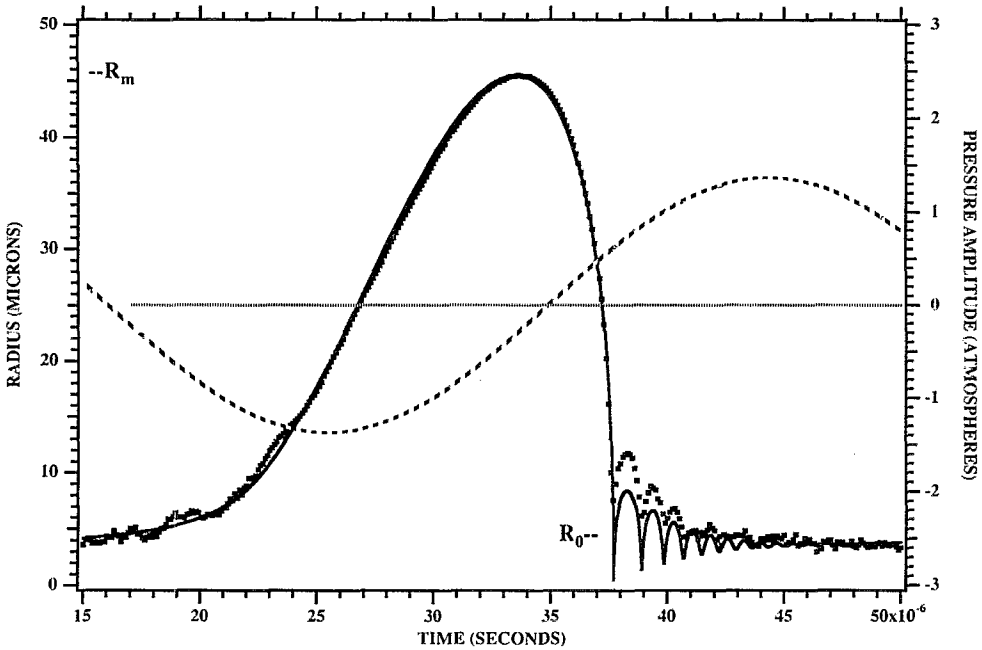

FIG. 1. The radius of an air bubble in water as a function of time for one cycle of the driving sound field. The dots are experimental data obtained by light-scattering from a sonoluminescing bubble. The solid line is a solution to the R–P equation (9) for $P_a=1.35$ atm, $\omega_a=2\pi$ (26.5 kHz), $R_0=4.5$ μm, $\rho=1000$ kg/m^3, $c=1481$ m/sec, $\eta=0.003$ kg/m sec, and $\sigma=0.03$ kg/sec^2. The ambient radius R_0 corresponds to the bubble's size when the driving sound amplitude (shown by the dashed line) passes through its first node. In response to the rarefaction phase of the sound field the bubble grows to a maximum size R_m.

the region of collapse in Fig. 1. The asymmetry of the bubble's expansion and collapse is the key to sonoluminescence. During the slow expansion the bubble absorbs sound energy from the drive, which is subsequently concentrated by the dramatic collapse to the length and time scales characterizing the hard core minimum.

In the standard model of SL the light emission is a secondary effect, due to dramatic adiabatic compression of

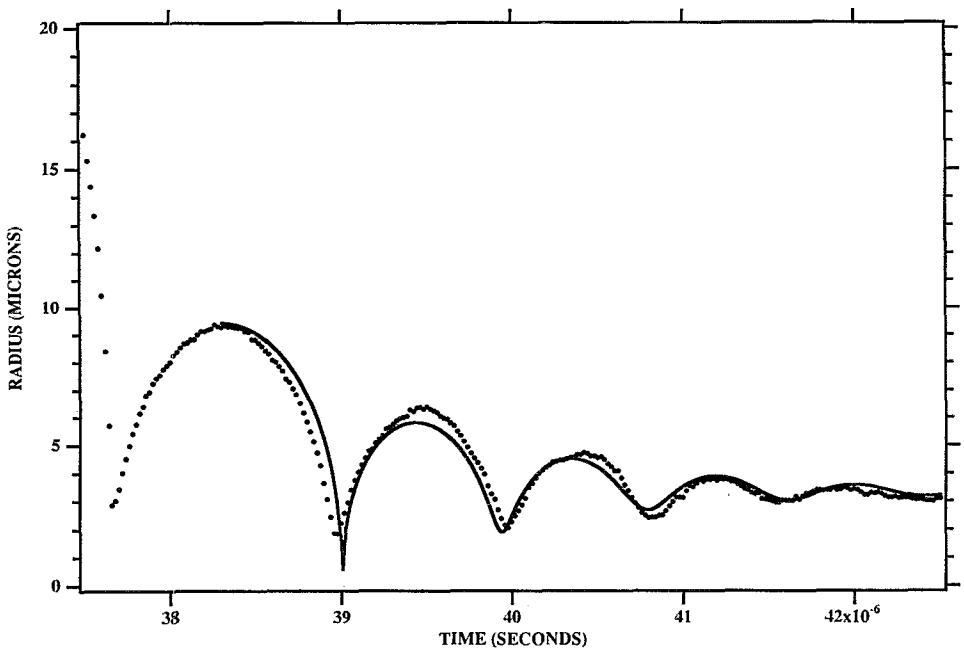

FIG. 2. Details of the bouncing behavior of the bubble following the collapse. The dots are experimental data. The solid line is a solution to (9) with an isothermal equation of state for the parameters of Fig. 1.

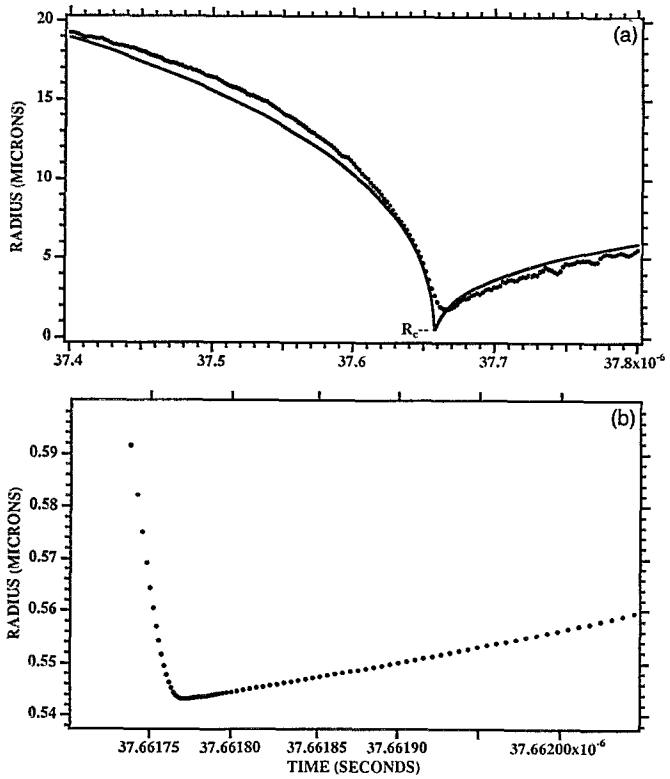

FIG. 3. Detailed blowup of the collapse region. In (a) the dots are experimental data and the solid line is a solution to (9) for the parameters of Fig. 1; (b) is a magnification of the region around R_c, the theoretical minimum radius, showing the time scale of the turnaround.

the bubble contents. As the bubble collapses, the gas inside reaches temperatures and pressures sufficiently intense to cause incandescence[6] or molecular excitation and recombination (chemiluminescence).[7] In these models the characteristics of the light pulses are directly correlated to the bubble dynamics: the duration of the minimum radius "hot spot," Δt_c, determines the length of the light flashes, and the temperature and pressure at this minimum radius, T_c and P_c, determine the spectral features and intensity of the light. For the motion in Fig. 1, this model predicts a peak temperature of 8500 K, corresponding to a blackbody spectral peak of 340 nm.

A problem with the standard model of SL as outlined above is made apparent by Fig. 4, which shows the Mach number, M_g, of the bubble wall relative to the speed of sound in the gas. It is clear that for these parameters M_g exceeds unity, in contradiction to the requirement $M_g^2 \ll 1$, which, as shown in the Introduction and Appendix B, must be obeyed in order to use (2) (where P_g is independent of r inside the bubble) to solve (1). To make matters even more interesting we see that solutions that probe shorter time scales and hotter emissions require even larger Mach numbers.

Nevertheless, hydrodynamics still describes the preliminary stages of the energy-focusing phenomena, including the "recharge" of the bubble by the sound field and the runaway collapse, which, in turn, set up the conditions for the emission of an imploding shock. Figures 1–3, in fact, indicate that the validity of the low Mach number hydrodynamic description is rather remarkable. Shown on these figures is the measured bubble radius as a function of time as determined by light scattering.[8] It is only during the

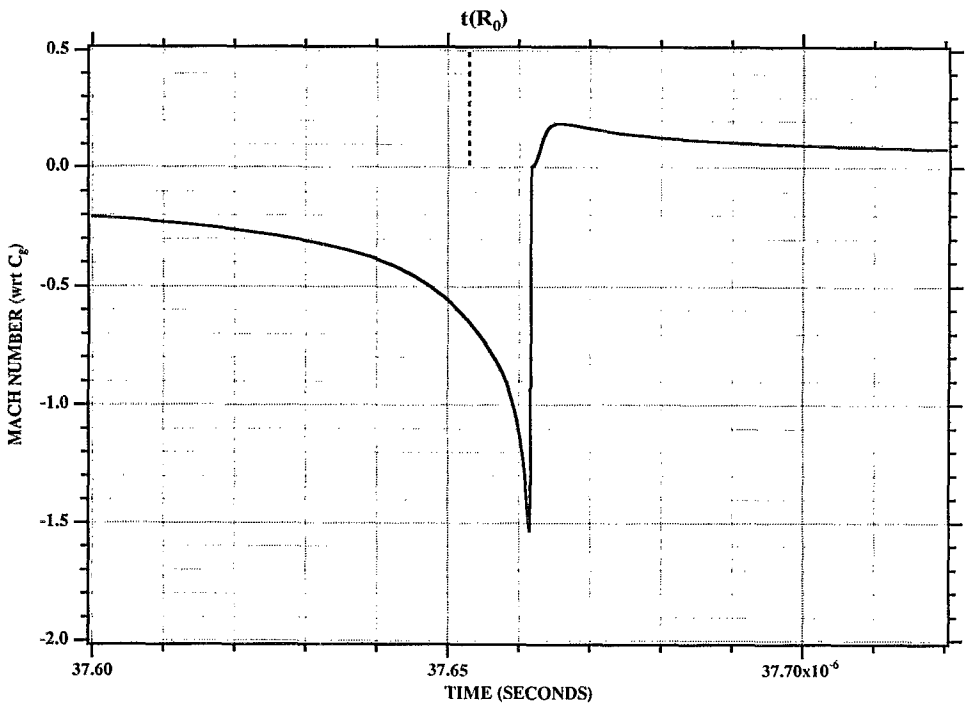

FIG. 4. The Mach number of the bubble wall relative to the instantaneous speed of sound in the bubble. Indicated on the figure is $t(R_0)$, the time at which the bubble passes through its ambient radius.

very last stages of collapse (0.03% of the acoustic cycle) that the simple model (1) shows any significant deviation from experiment. In fact, the subsonic motion predicted by the R–P equation has been used to calibrate experimental radius-versus-time curves.[8]

In view of the many experimental features of high-amplitude bubble motion and inferred characteristics of SL that are at least qualitatively described by (1), we set out to derive scaling laws for the bubble motion based upon the standard model. These dimensional relations connecting various aspects of the bubble dynamics will hopefully point the way in parameter space toward greater energy focusing and shorter flash widths, although the first principles model of SL will surely require refinement.

To broach analysis of the bubble's nonlinear oscillation we isolate a set of key variables characterizing its motion. The rarefaction expands the bubble from its ambient size, R_0, to its maximum, R_m; the maximum is reached at a phase φ_m relative to the sound field. The subsequent collapse to the minimum radius, $R_c = a + \delta R_c$, is characterized by the turnaround time Δt_c and temperature and pressure, T_c and P_c, given by (2). To obtain relations for these variables we distinguish various aspects of the bubble motion and in these regimes use appropriate approximations to simplify the R–P equation. The resultant scaling laws contain coefficients that are specified by comparison to a particular numerical simulation, with the assumption that variations in these coefficients with the drive parameters are higher-order effects. Here in the Introduction are presented only the simplest forms of these laws; their derivations and possible refinements and a discussion of their usefulness and limitations is relegated to the relevant sections.

At the maximum rarefaction of the drive pressure the expansion of the bubble is linear with time (Fig. 1); this extended region of linear growth is used to derive scaling relations for R_m and φ_m. By estimating the duration of this linear expansion and evaluating its slope from the R–P equation, the maximum is given by

$$R_m = R_0 + \frac{\pi \zeta'}{\omega_a}\left(\frac{2}{3}\frac{P_a' - P_0}{\rho}\right)^{1/2}, \tag{3}$$

where P_a' is the drive amplitude, ω_a is the acoustic frequency, and $\zeta'(\approx 0.42)$ is a scaling factor of order unity to be found by matching (3) to a single simulation. The increasing external pressure and the size-dependent inertia of the bubble finally halt the bubble's growth. We approximate a first integration of the R–P equation about the region of linear growth and then find the time corresponding to zero velocity. The phase of the maximum relative to the driving sound field (measured relative to the node preceding the compression) then satisfies

$$\left(\frac{P_0}{\rho} + \frac{1}{2}\alpha^2\right)\left(\frac{\pi}{2} - \varphi_m\right) - \frac{P_a \cos\varphi_m}{\rho} = \frac{R_m \omega_a \alpha}{2}, \tag{4}$$

where $\alpha \equiv [2(P_a' - P_0)/3\rho]^{1/2}$ is the velocity in the linear growth region. The key time scale associated with the collapse and hot spot lifetime, Δt_c, is derived by expanding the R–P equation about the minimum radius. The resultant harmonic oscillator solution defines a frequency associated with the hard core collapse, whence

$$\Delta t_c = \pi 3^{\gamma/2}\frac{a}{c_0}\left(\frac{\rho a^3}{\rho_0 R_0^3}\right)\left(\frac{a}{R_0}\right)^{3(\gamma-1)/2}\left(\frac{\delta R_c}{a}\right)^{(\gamma+1)/2}, \tag{5}$$

where c_0 is the speed of sound in the gas and ρ_0 is the gas density at T_0 and P_0. Finally, by considering a first integration of the R–P equation we obtain an energy equation for the bubble's motion. Steady-state oscillations require that the net change in the kinetic and potential energies of the fluid and gas during a cycle be zero. Equating the work done by the sound field as the bubble expands to the sound radiated by the bubble as it accelerates during the collapse yields the relation between maximum and minimum:

$$\frac{4\pi^2}{\gamma 3^{3\gamma/2}} P_0 a^3 \frac{c_0}{c}\left(\frac{R_0}{a}\right)^{9\gamma/2}\left(\frac{a}{\delta R_c}\right)^{(3\gamma-1)/2}\left(\frac{\rho_0}{\rho}\right)^{1/2} = \frac{8\pi}{3} P_a R_m^3 \cos\varphi_m \sin\Delta, \tag{6}$$

where $\sin\Delta(\approx 0.34)$ is the scaling factor again to be determined by matching (6) to a single simulation.

The above relations (2)–(6) are a complete set of equations for the conditions of the collapse as functions of the drive parameters, P_a, ω_a, and R_0, as implied by the R–P equation. A discussion of heat conduction and a refinement of the purely adiabatic equation of state in Sec. V emphasizes the generality of our analysis. A determination of the as yet arbitrary theoretical parameter R_0 requires input beyond the R–P equation. We consider mass diffusion into and out of the bubble as a mechanism for determining R_0. Since the synchronous SL experiments use degassed fluids, the quiescent or linearly oscillating bubble will dissolve into the fluid. However, the asymmetry of the bubble's nonlinear motion can prevent the bubble from dissolving by allowing mass to flow into it during the expansion phase when the partial pressure in the bubble is lower than the partial pressure to which the fluid is degassed. Requiring that the net mass flow across the bubble surface per cycle be zero yields

$$R_0 = \xi\left(\frac{P_\infty}{P_0}\right)^{1/3} R_m, \tag{7}$$

where P_∞ is the partial pressure of the gas above the fluid and ξ is a constant of order unity. In Sec. V we develop a systematic procedure to couple the equations of mass diffusion and bubble dynamics to establish a steady state. Comparison of experiment and theory yield consistent results for high-amplitude bubble motion below the SL threshold. The application of the procedure to the SL regime of bubble motion, however, indicates that the steady-state solution is determined by processes unaccounted for in our simple model.

Returning to Fig. 1, we note the presence of two periodicities. On the one hand, the bubble recharges and collapses once for each acoustic cycle. On the other hand, the collapse is followed by bouncing with a periodicity that is

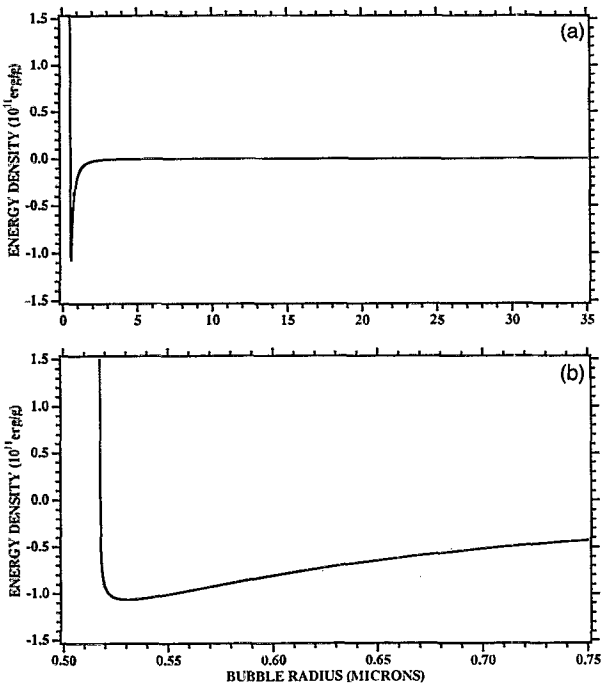

FIG. 5. The potential well corresponding to the bubble's motion in the Hamiltonian limit. The radius of the bubble moves like a ball of unit mass rolling in this potential (23). The relevant parameters are $P_\infty = 1$ atm, $R_m = 38$ μm, $R_0 = 4.5$ μm, and $\rho = 1000$ kg/m^3; (b) is an expanded picture of the minimum of (a).

much shorter than that of the sound field, as is shown in detail by Fig. 2. This latter time scale is made apparent by rewriting (1) in its Hamiltonian limit as an equation for the motion of a particle in a potential well (Sec. III). The potential well picture of the bubble motion also provides an insight into the energy-focusing properties of the bubble, The potential (Fig. 5) shows clearly how at the maximum radius the bubble is accelerating very slowly, while at the minimum point of the collapse the acceleration is increased by a factor of 10^{10}.

The enormous acceleration at the minimum leads to a radiation of sound from the bubble surface into the fluid. Despite the small size of the bubble the nonlinear oscillations so efficiently absorb and reradiate the sound energy of the drive that, for reasonable parameters, this radiation can dominate the quality factor of the entire resonator (Sec. IV).

In the first section we shall derive the R–P equation from the basic equations of fluid mechanics, with an emphasis on the underlying assumptions and limitations. In particular, the relevant constraints on the bubble motion include that the Mach numbers in the fluid and gas be small, i.e.,

$$\frac{\dot{R}}{c} \ll 1, \quad \frac{\dot{R}}{c_0} \ll 1. \tag{8}$$

The evident violation of these conditions for drive parameters characterizing the experiments indicates the necessity of including nonlinear wave motion and shock waves in a more refined analysis. The mathematical conditions for breakdown of equilibrium in the gas are presented in Appendix B and the implications for theoretical work discussed in Sec. VII.

As we have seen, the R–P equation is an accurate description of most of the cycle of the bubble's oscillation and shows how the nonlinear motion effectively concentrates the diffuse energy of the drive. But, despite the low Mach numbers of the imposed sound field, the R–P equation does not suffice to describe SL, because the hydrodynamics spontaneously creates regions near the bubble with Mach numbers approaching (or exceeding) unity. In this way the mathematical basis of the derivation of the R–P equation is violated as the bubble collapses. However, this points the way to the refinements needed to extend the region of applicability of the theory. The Mach numbers reached by the collapsing bubble necessitate the inclusion of shock wave formation, the extremes of temperature and pressure inside the bubble suggest ionization of its contents, and the spatial scales characterizing the minimum size of the bubble, comparable to the wavelength of the emitted radiation, raise questions regarding cooperative emission processes as well as effects due to the density of states in confined geometries.[9]

Despite the desirable theoretical refinements that would be necessary to provide a complete description of bubble motion and light emission, the R–P equation still constitutes a phenomenological picture of SL, and thus provides an essential practical connection between theory and experiment. On a grander scale, this model may even serve as a prototype for energy focusing in other systems.

II. THE RAYLEIGH–PLESSET EQUATION FOR BUBBLE OSCILLATIONS IN A COMPRESSIBLE FLUID

The Rayleigh–Plesset equation provides the leading-order description of the breathing motion of a gas-filled bubble driven by a sound field. When modified to include the radiation of acoustic energy from the bubble to the fluid, this fundamental equation takes the form

$$-R\ddot{R}\left(1-\frac{2\dot{R}}{c}\right)-\frac{3}{2}\dot{R}^2\left(1-\frac{4}{3}\frac{\dot{R}}{c}\right)+\frac{P(R,t)}{\rho}+\frac{R}{\rho c}\frac{dP(R,t)}{dt}$$
$$-\frac{P_a(0,t)}{\rho}-\frac{R}{\rho c}\frac{dP_a(0,t)}{dt}-\frac{P_0}{\rho}=0, \tag{9}$$

supplemented by the boundary condition at the fluid–gas interface,

$$P(R,t)+\frac{4\eta\dot{R}}{R}+\frac{2\sigma}{R}=P_g(R,t). \tag{10}$$

In these equations $R(t)$ is the radius of the bubble, c is the speed of sound in the fluid, ρ is the fluid density, $P(r,t)$ is the pressure in the fluid, $P_a(r,t)$ is the acoustic drive pressure, P_0 is the constant ambient pressure above the liquid, $P_g(r,t)$ is the pressure in the gas, η is the shear viscosity of the fluid, σ is the coefficient of surface tension, and the origin of the spherical coordinate system is located at the center of the bubble.

To complete the equations above, we specify the equation of state of the expanding and contracting bubble. We choose an adiabatic gas including the effect of the van der Waals hard core, since, as previously shown, for realistic drive parameters the bubble can collapse to sizes approaching the excluded molecular volume. Such a gas is characterized by the following equations:

$$P_g(R)=\frac{P_0R_0^{3\gamma}}{(R^3-a^3)^{\gamma}};\quad T_g(R)=\frac{T_0R_0^{3(\gamma-1)}}{(R^3-a^3)^{\gamma-1}},$$
$$c_g^2(R)=\frac{c_0^2R_0^{3(\gamma-1)}R^6}{(R^3-a^3)^{\gamma+1}};\quad \frac{dP_g(R)}{dR}=\frac{-3\gamma R^2P_0R_0^{3\gamma}}{(R^3-a^3)^{\gamma+1}}, \tag{11}$$

where $\frac{4}{3}\pi a^3$ is the van der Waals excluded volume ($=0.04$ l/mole for air), γ is the ratio of specific heats c_P/c_V, evaluated in the ideal gas limit ($=\frac{5}{3}$ for monatomic gases, $\frac{7}{5}$ for diatomic gases; $\gamma=1$ corresponds to an isothermal equation of state), R_0 is the radius at which the bubble contents are at ambient pressure, $P_0=1$ atm, and temperature, $T_0=300$ K ($R_0/a=8.54$ for air), and c_0 is the speed of sound in the gas at these conditions. The ambient radius is an unspecified theoretical parameter in the bubble equations.

The applicability of the R–P equation to bubble dynamics is limited by several approximations underlying its derivation. In particular, the imposed sound field must satisfy the condition

$$v/c\ll 1 \quad \text{(condition I)},$$

where v is the velocity amplitude of the sound wave, viz. that the Mach number of the imposed sound field is small. Also, the wavelength of the driving field should be large compared to the radius of the bubble,

$$kR\ll 1 \quad \text{(condition II)},$$

where k is the wave number of the sound field. Further, the analysis requires that the motion of the bubble wall be slow compared to the speed of sound in the fluid,

$$\frac{\dot R}{c}\ll 1;\quad \frac{R\ddot R}{c^2}\ll 1 \quad \text{(condition III)},$$

and compared to the (instantaneous) speed of sound in the gas,

$$\frac{\dot R}{c_g}\ll 1;\quad \frac{R\ddot R}{c_g^2}\ll 1 \quad \text{(condition IV)}.$$

The roles of these approximations are elucidated by the derivation of (9) that follows.

For sufficiently low-amplitude motion (condition I), the velocity potential in the fluid satisfies the wave equation[10]

$$\nabla^2\varphi(\mathbf{r},t)-\frac{1}{c^2}\frac{\partial^2}{\partial t^2}\varphi(\mathbf{r},t)=0. \tag{12}$$

We write the velocity potential as

$$\varphi=\varphi_{\text{in}}+\varphi_{\text{sc}},$$

the sum of incident and scattered wave fields. As the driving field we assume a plane standing wave,

$$\varphi_{\text{in}}=A\sin kz\cos\omega t, \tag{13}$$

where A is the amplitude and ω is the drive frequency. The analysis that follows is readily adapted to other incident wave geometries in the long-wavelength limit. We rewrite the coordinate as

$$z=z_0+r\cos\theta$$

where z_0 is the location of the bubble's center. For $kR\ll 1$ (condition II) the monopole component of φ_{in} dominates, and the motion of the bubble is purely radial. Near the bubble the incident velocity potential is[11]

$$\varphi_{\text{in}}=A\sin kz_0\cos\omega t(1-\tfrac{1}{6}k^2r^2)+O(k^4r^4), \tag{14}$$

and the radially symmetric velocity component for small r is

$$\nabla\varphi_{\text{in}}=-\frac{A}{3}k^2r\sin kz_0\cos\omega t. \tag{15}$$

The scattered velocity potential is in the form of an outgoing spherical wave originating at $r=R(t)$, the surface of the bubble. We write

$$\varphi_{\text{sc}}=\frac{g[t-(r-R)/c]}{r}-\frac{R}{cr}g'\left(t-\frac{r-R}{c}\right), \tag{16}$$

which satisfies the wave equation (12) given the constraints of condition III. The function g is determined by applying the boundary condition

$$\left(\frac{\partial\varphi(r,t')}{\partial r}\right)_{r=R}=\dot R(t'). \tag{17}$$

For $kR\ll 1$ (condition II) and sufficiently slow bubble wall velocities (condition III),

$$\varphi_{\text{sc}}(r,t)=\left(\frac{-R^2\dot R}{r}+\frac{R}{cr}(R^2\ddot R+2R\dot R^2)\right)_{t'=t-(r-R)/c}, \tag{18}$$

evaluated at the retarded time.

Neglecting the effect of thermal conductivity, Bernoulli's equation for the fluid is

$$h(\infty,t)-h(R,t)=\frac{P(\infty,t)-P(R,t)}{\rho}$$
$$=\left(\frac{\partial\varphi}{\partial t}+\frac{(\nabla\varphi)^2}{2}\right)_{r=\infty}$$
$$-\left(\frac{\partial\varphi}{\partial t}+\frac{(\nabla\varphi)^2}{2}\right)_{r=R}, \tag{19}$$

where $h(r,t)$ is the enthalpy of the fluid. Using the expressions (14) and (18) for φ in (19) yields the equation

$$-R\ddot{R}-\frac{3}{2}\dot{R}^2+\frac{\dot{R}}{c}(6R\ddot{R}+2\dot{R}^2)+\frac{R^2\ddot{R}}{c}+\frac{P(R,t)}{\rho}-\frac{P_a(0,t)}{\rho}$$

$$-\frac{P_0}{\rho}=0, \tag{20}$$

where $P_a(0,t)$ is the acoustic pressure at the location of the bubble. Solving the incompressible limit of (20) for $\ddot{R}$ and substituting it into (20) yields the final form of the R–P equation (9). The pressures in the fluid and the gas are related as in (10) by equating the radial components of the stress tensors at the bubble surface.

In specifying the behavior of the bubble contents as in (11) we have suppressed the radial dependence of $P_g(r,t)$, assuming that it is uniform inside the bubble. This assumption holds true when the quantities $\dot{R}/c_g$ and $R\ddot{R}/c_g^2$ are small, so that the time scale for equilibration of the bubble contents is small compared to that governing the bubble's motion (condition IV). The breakdown of this local equilibrium signals the formation of shock fronts that are beyond the scope of this analysis (cf. Sec. VII and Appendix B). In addition, the equation of state (11) assumes a constant number of molecules in the bubble throughout its oscillation; i.e., we neglect the effects of evaporation/condensation and mass diffusion (cf. Sec. VI and V).

Equation (9) is the basis for the bubble motion figures shown in the Introduction. This equation includes damping effects that arise from viscosity and the radiation of sound at the bubble/fluid interface.

III. ENERGY LAW FOR BUBBLE MOTION

The essential characteristics of the bubble motion are made apparent by the energy equation that is obtained from a first integration of (9). Multiplying (9) by $4\pi\rho\dot{R}R^2$ yields

$$\frac{d}{dt}\left[2\pi\rho R^3\dot{R}^2\left(1-\frac{4}{3}\frac{\dot{R}}{c}\right)+\frac{4\pi}{3}\frac{P_0R_0^{3\gamma}}{(\gamma-1)(R^3-a^3)^{\gamma-1}}+\frac{4\pi}{3}R^3[P_0+P_a(0,t)]\right]$$

$$=\frac{4\pi}{3}R^3\frac{dP_a(0,t)}{dt}+\frac{4\pi}{c}R^3\dot{R}^2\frac{dP_g(R)}{dR}-\frac{4\pi}{c}R^3\dot{R}\frac{dP_a(0,t)}{dt}-16\pi\eta\dot{R}^2R, \tag{21}$$

where surface tension has been dropped, its contribution to the energy being small in all cases of interest.[12] In (21) the lhs consists of the kinetic and potential energy of the fluid and the potential energy of the gas. The rhs includes the changes in the energy of the system due to the work done on the bubble by the driving sound field, the sound radiated by the oscillating bubble into the fluid (these terms include the factor $\dot{R}/c$), and the heat dissipated by the fluid's viscosity.

In the Hamiltonian limit, neglecting viscous and radiation losses, Eq. (21) reduces to that of a particle of unit mass rolling in a potential well. The corresponding Hamiltonian[13] is

$$H=\left(\frac{\dot{R}^2}{2}+\frac{P_0R_0^{3\gamma}}{3(\gamma-1)R^3(R^3-a^3)^{\gamma-1}\rho}+\frac{P_0+P_a(t)}{3\rho}\right), \tag{22}$$

where $P_a(t)\equiv P_a(0,t)$. In particular, to model the dynamics of the collapse from R_m to R_c, we can neglect the variation in acoustic pressure on the time scale of the bubble's motion and set the rhs of (21) equal to zero. The equation of motion then reduces to

$$\frac{\dot{R}^2}{2}+\frac{P_0R_0^{3\gamma}}{3(\gamma-1)R^3(R^3-a^3)^{\gamma-1}\rho}+\frac{P_\infty}{3\rho}+\frac{E_0}{R^3}=0, \tag{23}$$

where $P_\infty=P_0+P_a[t(R_m)]$ and the integration constant, E_0, is fixed by the condition $\dot{R}(R_m)=0$.

Equations (22) and (23) provide an interpretation of the various time scales that characterize the bubble motion. First, there is the overall periodicity or repetition rate of the phenomenon, which is determined by the frequency of the driving sound field $P_a(t)$. Second, the turnaround time at the minimum (or collapse) radius is given by

$$\left(\frac{R_c}{\ddot{R}_c}\right)^{1/2}\sim\left[3^\gamma\frac{\rho a^2}{P_0}\left(\frac{a}{R_0}\right)^{3\gamma}\left(\frac{\delta R_c}{a}\right)^\gamma\right]^{1/2}, \tag{24}$$

which for the parameters in Fig. 5 is a few picoseconds. The highly skewed shape of the potential well accounts for the asymmetry in the bubble's motion. This asymmetry is demonstrated in the ratio of accelerations at the minimum and maximum radii,

$$\frac{\ddot{R}_c}{\ddot{R}_m}=\frac{1}{3^\gamma}\left(\frac{R_0}{a}\right)^{3\gamma}\frac{R_m}{a}\left(\frac{a}{\delta R_c}\right)^\gamma\frac{P_0}{P_0+P_a\sin\varphi_m}, \tag{25}$$

which is $\sim 10^{10}$ for the parameters under consideration.

The third time scale associated with the motion in Fig. 1 is the time between the successive minima following R_c. This is determined by the slow expansion and contraction of the bubble as it passes through a relative maximum in radius. This period scales as

$$\left(\frac{R_m}{\ddot{R}_m}\right)^{1/2}=\left(\frac{R_m^2\rho}{P_0+P_a(\varphi_m)}\right)^{1/2}, \tag{26}$$

and is measured in microseconds. While the Hamiltonian limit implies repetitive oscillations between the same maximum and minimum radii, the amplitude of the bubble's motion will, in practice, depend on the external pressure (i.e., the potential well will distort in time). Also, the amplitude of the breathing motion will damp out significantly in time when viscous and radiative losses are taken into account. In the limit of small amplitudes of drive, the motion in the potential well reduces to the (adiabatic) radial resonant mode of the bubble.[14]

$$\omega_0^2=\frac{3\rho_g}{\rho}\frac{c_g^2}{R_0^2}. \tag{27}$$

IV. SCALING LAWS FOR HIGH-AMPLITUDE BUBBLE MOTION

The nonlinearities present in the R–P equation account for the richness of its solutions but also render intractable an exact analysis. As shown in Fig. 1 the bubble responds to a negative pressure swing by slowly expanding to a maximum radius. As the driving pressure turns positive the bubble collapses rapidly to its minimum size. This dramatic asymmetry between expansion and collapse makes SL possible.

In the traditional model of SL, the light emission is associated with the high temperatures and pressures characterizing the collapsed bubble. In this model the theoretical parameters relevant to the experiment are T_c, the maximum temperature of the bubble contents upon collapse, P_c, the maximum pressure inside the bubble, and Δt_c, the duration of these conditions; in the rudimentary hydrodynamic model this time is correlated with the duration of the light flashes.

In the hydrodynamic theory these quantities are functions of the external drive parameters, P_a and ω_a, and the theoretical parameter R_0. To obtain a qualitative interpretation of the bubble's high-amplitude motion, we consider separately various regimes of the bubble's steady-state oscillations. In each regime we isolate the dominant terms of the R–P equation; the resultant mathematical simplifications yield scaling laws for the characteristics of the bubble's oscillation including the parameters discussed above. The purpose of the scaling laws is not to give an exact solution for the bubble dynamics for any drive parameters. Rather, given the characteristics of the motion for particular experimental parameters, the scaling laws predict the changes in the quantities relevant to SL with variations of these parameters. By simplifying the mathematics the scaling laws provide insight into the nonlinear motion of the bubble, elucidate the dependence of this motion on the experimental conditions, and ultimately yield theoretical predictions regarding the bubble dynamics and SL to be tested in the laboratory.

First, we consider the expansion to R_m that occurs in response to the negative pressure swing of the drive. Clearly, as the bubble expands, the gas pressure inside it becomes smaller and sufficiently far into the expansion that term in the R–P equation may be dropped. Assuming that this criterion is met and neglecting the loss terms that are small during the slow expansion, we expand the R–P equation (9) around the instant of maximum rarefaction of the drive:

$$R\ddot{R}+\frac{3}{2}\dot{R}^2=\frac{P'_a-P_0}{\rho}-\frac{P'_a}{\rho}\frac{\omega_a^2 t^2}{2}, \tag{28}$$

where $P_a(t) = -P'_a \cos \omega_a t$. Writing $R(t)$ as a power series in time shows that for small times the expansion is accurately linear; indeed the coefficients of both the quadratic and cubic terms in the series are identically zero. The leading-order solution for $R(t)$ is

$$R=R(0)+\alpha t-\delta t^4, \tag{29}$$

where

$$\alpha=\left(\frac{2}{3}\frac{P'_a-P_0}{\rho}\right)^{1/2}, \quad \delta=\frac{P'_a\omega_a^2}{24\rho R(0)},$$

and $R(0)$ is the radius at the time of maximum rarefaction taken here to be $t=0$. *A posteriori* it is clear that the analysis has validity only for drive amplitudes exceeding the ambient pressure. The linear expansion lasts for approximately the duration of the net rarefaction phase of the external pressure, $P_0+P_a(t)$, which is on the order of half an acoustic cycle. Note this effect in Fig. 1. Clearly the linear regime cannot be valid for R near R_0, since for such radii the gas pressure becomes an important effect. However, given the relatively rapid decrease in $P_g(R)$ with increased radius we neglect the precise dynamics of the bubble's expansion near R_0 and assume that the linear growth regime is quickly reached. For R_m we then obtain the following scaling law:[15]

$$R_m=R_0+\zeta'\frac{\pi}{\omega_a}\left(\frac{2}{3}\frac{P'_a-P_0}{\rho}\right)^{1/2}, \tag{30}$$

where the constant ζ' is to be obtained from the computed solution of (9) for specific parameters and is of order unity.

The expression above, although it gives a good ($\pm 20\%$) leading-order estimate of the maximum radius, can be refined by a consideration of the phase of the bubble's response relative to the driving field. Depending on the drive parameters and the size of the bubble, the inertia of the bubble will determine how soon after the end of the net pressure rarefaction the bubble will begin to collapse. Taking this effect into account, we can write, instead of (30),

$$R_m=R_0+\left(\frac{\zeta\pi}{\omega_a}+\frac{\varphi_m}{\omega_a}\right)\left(\frac{2}{3}\frac{P'_a-P_0}{\rho}\right)^{1/2}, \tag{31}$$

where ζ is a (different) constant still of order unity. In (31) the phase of the maximum φ_m is measured relative to the node before the compression phase of the drive pressure. A positive phase implies that the bubble continues to grow even for positive drive pressures and negative φ_m indicates a shorter expansion.

To find the phase of the maximum we can rewrite (9), neglecting $P_g(R)$ and the dissipative terms, as

$$\frac{d}{dt}\left(R\dot{R}+\frac{P_0 t}{\rho}-\frac{P'_a}{\rho\omega_a}\sin\omega_a t-R(0)\alpha\right)=\frac{-1}{2}G\dot{R}^2, \tag{32}$$

where $t=0$ corresponds to the instant of maximum pressure rarefaction. When $G=1$, (32) is the R–P equation appropriate to the bubble's expansion; when $G=0$ the equation has an exact solution, where the integration constant is fixed by the initial conditions $R(t=0)=R(0)$ and $\dot{R}(t=0)=\alpha$. We approximate the integration of the R–P equation by exploiting the extended region of linear growth and setting $\dot{R}=\alpha$ on the rhs of (32) (with $G=1$). The error in the integration is then limited by the time during

which $\dot{R}$ deviates from the constant value. Using this approximation to integrate (32) and solving for the time at which $\dot{R}=0$, yields the following equation for the phase of the maximum (relative to the drive pressure node preceding the compression):

$$\left(\frac{P_0}{\rho}+\frac{1}{2}\alpha^2\right)\left(\frac{\pi}{2}-\varphi_m\right)-\frac{P_a'}{\rho}\cos\varphi_m=\frac{R_m\alpha\omega_a}{2}. \tag{33}$$

Here we have set $R(0)$, which for experimental parameters lies at the midpoint of the linear expansion phase, equal to $R_m/2$. Integrating (32) once more yields an equation for R_m whose dependence on the drive parameters for small φ_m agrees with that of (31). Estimating R_m by (30), solving (33) for φ_m, and then applying (31) yields a more accurate estimate of the maximum. For smaller amplitudes of drive pressure, i.e., $P_a' \approx P_0$ the expressions above become less valid. In this instance the initial expansion does not proceed rapidly enough to justify neglecting $P_g(R)$. In fact, the bubble's motion for $P_a' \lesssim P_0$ and $P_a' > P_0$ is fundamentally different as regards how the dynamics depends on the drive (cf. Sec. V).

For steady-state bubble motion, as should apply to the synchronously sonoluminescing bubble, the net energy change during a cycle of the bubble's motion is zero. Thus the rhs of (21) yields zero when integrated over one period of the sound field, i.e., the sound energy absorbed by the bubble from the drive is equal to the sound radiated by the bubble's motion in the fluid and the energy converted into heat by the fluid's viscosity. For the drive parameters appropriate to describing SL the collapses are sufficiently violent that the sound radiation dominates viscous losses; for the purposes of our scaling relations the viscous sink will be neglected. These energy considerations give a scaling law relating the characteristics of the expansion to those of the minimum radius.

The absorption of energy by the bubble from the sound field scales with the bubble's volume and is thus dominated by large R. To estimate the energy absorbed, we approximate the R–P equation (9) by expanding around the maximum radius:

$$R=R_m+\delta R, \quad \text{where } \delta R \ll R_m.$$

Integrating the resultant equation [where for these large R the $P_g(R)$ term has been dropped and $t=0$ corresponds to the pressure node preceding the compression phase],

$$R_m\,\delta\ddot{R}=-\frac{1}{\rho}(P_0+P_a\sin\omega t), \tag{34}$$

subject to the constraints that $\delta\dot{R}(t_m)=0$ and $\delta R(t_m)=0$ yields, for small $\Delta t=(t-t_m)$,

$$\delta R=\frac{1}{\rho R_m}\left(\frac{1}{2}(P_0+P_a\sin\varphi_m)(\Delta t)^2 + \frac{P_a\omega}{6}\cos\varphi_m(\Delta t)^3\right). \tag{35}$$

The sound energy input during the expansion of the bubble is then

$$\frac{4\pi}{3}\int_{t_m-\Delta/\omega_a}^{t_m+\Delta/\omega_a} R^3\frac{dP_a}{dt}\,dt=\frac{8\pi}{3}R_m^3P_a\cos\varphi_m\sin\Delta + O(\Delta^3). \tag{36}$$

Here Δ represents the width of the integration that is determined by matching to a simulation and is small enough so that higher-order terms in (36) can be neglected. Indeed, when φ_m is sufficiently small, so that the maximum radius is reached close to the drive pressure node, the maxima of R^3 and dP_a/dt are nearly in phase and the integral in (36) is sharply peaked.

The sound emitted by the bubble, given by the second and third terms on the rhs of (21), is radiated predominately near R_c, where the bubble undergoes huge accelerations. To estimate the magnitude of the radiative terms of (21), we solve for $P_g(R)-P_a(t)$ in (9) and differentiate

$$\left\langle\frac{4\pi}{c}R^3\dot{R}\frac{d}{dt}(P_g-P_a)\right\rangle=\left\langle\frac{4\pi}{c}\rho R^4\ddot{R}^2\right\rangle, \tag{37}$$

where the brackets denote the time integral of the quantity inside for a cycle. The total sound radiated at the collapse is then

$$\frac{4\pi\rho}{c}\left(\frac{P_0R_0^{3\gamma}}{\rho}\frac{a}{(3a^2\,\delta R_c)^\gamma}\right)^2\Delta t_c. \tag{38}$$

Here the acceleration has been evaluated at the minimum radius [where the $P_g(R)$ term dominates the R–P equation], and Δt_c is the time that the bubble spends near the minimum. This time scale is found by expanding the R–P equation for $R=R_c+\delta R$:

$$a\,\delta\ddot{R}+\left(\frac{1}{\rho}\frac{dP_g}{dR}\right)_{R=R_c}\delta R=\frac{P_g(R_c)}{\rho}. \tag{39}$$

Choosing $\delta R=0$ at $t=0$, the time of minimum radius, yields

$$\delta R=\left|\frac{P_g(R_c)}{(dP_g/dR)_{R=R_c}}\right|\left(1-\cos\frac{\pi t}{\Delta t_c}\right), \tag{40}$$

where the time scale of the turnaround is

$$\Delta t_c=\pi\left(\frac{\rho a}{|(dP_g/dR)_{R=R_c}|}\right)^{1/2} =\pi 3^{\gamma/2}\frac{a}{c_0}\left(\frac{\rho a^3}{\rho_0R_0^3}\right)^{1/2}\left(\frac{a}{R_0}\right)^{3(\gamma-1)/2}\left(\frac{\delta R_c}{a}\right)^{(\gamma+1)/2}. \tag{41}$$

The scaling relation between R_m and R_c is then given by equating (36) and (38), using Δt_c defined above,

$$\frac{4\pi^2}{\gamma 3^{3\gamma/2}}P_0a^3\frac{c_0}{c}\left(\frac{R_0}{a}\right)^{9\gamma/2}\left(\frac{a}{\delta R_c}\right)^{(3\gamma-1)/2}\left(\frac{\rho_0}{\rho}\right)^{1/2} =\frac{8\pi}{3}P_aR_m^3\cos\varphi_m\sin\Delta, \tag{42}$$

where $\sin\Delta$ is the constant to be matched to simulation. The scaling relations (31), (33), and (42) provide a com-

TABLE I. Variation of the characteristics of bubble motion as determined by scaling laws (31), (33), and (42). The parameters of Fig. 1 are used to predict the motion when (a) the acoustic pressure amplitude is increased and (b) the ambient radius is increased.

	R_0	P_a	R_m	ϕ_m	R_c	Δt_c	T_c
	4.5 μm	1.35 atm	43 μm	−0.27	0.523 μm	90 psec	8 500 K
(a)	4.5 μm	1.50 atm	57 μm	−0.08	0.531 μm	44 psec	11 000 K
(b)	6.0 μm	1.35 atm	46 μm	−0.23	0.741 μm	200 psec	7 100 K

plete characterization of the collapse parameters T_c, P_c, and Δt_c in terms of R_0 and the drive parameters P_a and ω_a.

As an example of the application of these scaling laws we first find the values of the scaling factors by matching to the theoretical curve in Fig. 1. For those drive parameters the characteristics of the bubble motion yield the following constants: in (33) $\zeta=0.51$, and in (42) $\sin\Delta=0.34$. Now we use the scaling laws to investigate the effects on the bubble motion of varying the external parameters. Table I shows the values of the key characteristics of the bubble motion for the conditions simulated in Fig. 1 and the corresponding values calculated using the scaling laws for the motion when (a) the drive amplitude P_a is increased and (b) when the ambient radius is increased.

The analysis of the minimum radius also provides a description of other aspects of the collapsing bubble. From (40) we can estimate the velocity of the bubble wall as the minimum is approached,

$$|\delta\dot{R}|_c=\frac{c_0}{\gamma 3^{\gamma/2}}\left(\frac{\rho_0 R_0^3}{\rho a^3}\right)^{1/2}\left(\frac{R_0}{a}\right)^{3(\gamma-1)/2}\left(\frac{a}{\delta R_c}\right)^{(\gamma-1)/2}. \tag{43}$$

The Mach numbers of the bubble wall relative to the fluid and gas follow from (43) and the equation of state. At the minimum, the Mach number in the liquid is

$$M_{lc}=\frac{|\delta\dot{R}|_c}{c}=\frac{c_0}{c}\frac{1}{\gamma 3^{\gamma/2}}\left(\frac{R_0}{a}\right)^{3(\gamma-1)/2}\left(\frac{a}{\delta R_c}\right)^{(\gamma-1)/2}\left(\frac{\rho_0 R_0^3}{\rho a^3}\right)^{1/2}, \tag{44}$$

and the Mach numbers relative to the speed of sound in air at ambient conditions c_0 is

$$M_{0c}=\frac{|\delta\dot{R}|_c}{c_0}=\frac{1}{\gamma 3^{\gamma/2}}\left(\frac{a}{\delta R_c}\right)^{(\gamma-1)/2}\left(\frac{R_0}{a}\right)^{3(\gamma-1)/2}\left(\frac{\rho_0 R_0^3}{\rho a^3}\right)^{1/2}. \tag{45}$$

The velocity of the bubble wall apparently increases as the collapse becomes more violent. Since the speed of sound in the bubble increases sharply as the contents are compressed, the instantaneous Mach number $M_g\equiv\dot{R}/c_g(R)$ at the minimum decreases for more violent collapses. However, M_g may have its maximum value before the bubble is at its minimum size, at some radius where the speed of sound is lower. For experimental parameters (e.g., those in Fig. 1), this radius is substantially larger than R_c, where radiation losses are important, and therefore the potential well model applies. Using $\dot{R}$ as given by (23) and $c_g(R)$ from (11), one can find the radii where (a) M_g is a maximum, and (b) M_g becomes unity. These are the radii at which to invoke condition IV (Sec. II) and the implications of its violation (cf. Sec. VII and Appendix B).

The expression (38) for the sound radiated by the bubble can also be used to calculate this contribution to the quality factor of the bubble's oscillation. In general, the quality factor for the whole system is given by

$$\frac{1}{Q_{\text{total}}}=\sum_i\frac{1}{Q_i},$$

where the Q_i's include thermal, viscous, and radiation damping of the bubble's motion and the dissipation associated with the larger experimental system of flask, piezolectric drive, etc. Formally the quality factor is defined as[16]

$$Q=\frac{2\pi(\text{energy of system at resonance})}{(\text{energy dissipated per cycle})}. \tag{46}$$

The sound energy of a spherical flask driven in its fundamental radial mode is given by

$$\left\langle\int_0^{R_f}\rho v^2\,d^3r\right\rangle=\int_0^{R_f}\rho k^2A^2j_0^2(kr)4\pi r^2\,dr\langle\cos^2\omega t\rangle=\pi\rho A^2R_f, \tag{47}$$

where the brackets represent the time average over a cycle, R_f is the radius of the flask, $A=P_a'/\rho\omega$, where P_a' is the amplitude of the pressure swing, and j_0 is the fundamental spherical Bessel function. The wave number k is determined by requiring that the pressure,

$$P_a(t)=P_a'j_0(kr)\sin\omega t,$$

satisfy the pressure release boundary condition at $r=R_f$. The Q due to the bubble is then given by the ratio of (47) to (38),

$$Q_b=\frac{\gamma^3}{2\pi}\left(\frac{P_a'}{\rho c^2}\right)^2\left(\frac{R_f}{a}\right)^3\left(\frac{1}{M_l(R_c)}\right)^3\frac{\delta R_c}{a}.$$

For typical experiments, the ratio $R_f/a\sim10^4$, $P_a'/\rho c^2\sim10^{-4}$, $M_l(R_c)\sim1$, and $\delta R_c/a\sim10^{-2}$, so $Q_b\sim10^2$–10^4. Despite the bubble's small size at the minimum and the brief duration of the hard core collapse, the sound energy radiated by the bubble is significant. In fact, under the assumption that the sound radiated by the bubble is lost to infinity, the theory suggests that the Q of the whole system can be limited by the violent collapse of the oscillating

bubble. Conversely, the lower bound on Q in the actual SL experiment here provides a clear check on the validity of the hydrodynamic theory. Indeed, as astonishing as the ability of the micron-sized bubble to focus the diffuse energy of the sound field to emit light is the intensity of the sound, it radiates into the fluid. Additionally, this property of the oscillating bubble provides for a precise comparison of theory to experiment, yielding insight into the mechanism of SL.

V. MASS DIFFUSION AND THE AMBIENT RADIUS

Since the collapse temperature is a strong function of the ambient radius, we now consider the physical criteria that determine R_0. In particular, we investigate the role of mass diffusion into and out of the oscillating bubble as the mechanism that determines the steady-state size of the bubble. Such an hypothesis is motivated by several observations. First, the stable SL demonstration can only be carried out in degassed water. (If the water is too air saturated, the acoustic sound energy is diffusely distributed among all the cavitation sites, and it is difficult to trap a bubble. When the bubble is trapped the mass flows into and out of it render its oscillation unstable.) A small stationary bubble in an undersaturated fluid will dissolve in about a second, while the stable sonoluminescing bubble can be maintained for hours. The nonlinear oscillation of the bubble counteracts its tendency to dissolve. Also, the solubility of air in water is anomalously low, about 30 times lower than that in CS_2, which is closest. Perhaps this is the condition that allows the air bubble to attain an SL steady state in water, whereas it has yet to be observed in another pure fluid.

To gain insight into how mass diffusion across the surface of a bubble undergoing high-amplitude breathing oscillations can prevent its dissolution, we separate the bubble's motion (Fig. 1) into two regimes. When the bubble is so large that the pressure of gas inside it is lower than the partial pressure to which the fluid is degassed, P_∞, mass will diffuse into the bubble from the solution. When the bubble is at its ambient size and smaller, there is a steady outflux of mass from the bubble into the undersaturated solution. Corresponding to the ambient (undersaturated) concentration of gas in the fluid, C_∞, one can define a radius R_∞ at which the pressure of air would be in thermodynamic equilibrium with the undersaturated fluid:

$$R_\infty = \left(\frac{C_0}{C_\infty}\right) R_0. \tag{48}$$

Qualitatively the physical mechanism that determines the ambient size of the oscillating bubble is the existence of an off-equilibrium steady-state mass outflux for $R < R_\infty$ and mass influx for $R > R_\infty$.

Experimentally, maintaining a bubble stably in a sound field requires a minimum drive pressure. In accordance with the mechanism sketched above the bubble's stability against dissolution depends on its expansion to a radius larger than R_∞. However, for small amplitudes of drive, i.e., $P_a' \lesssim P_0$, the bubble's motion can be linearized about R_0 as $R = R_0 + \delta R$, where $\delta R \lesssim R_0$. In this instance of linear or perturbed linear response the bubble will lose a fraction of its mass into the solution each cycle without a compensating mass influx and dissolve away. The mass flux through the surface of a bubble of radius R is given by

$$\frac{dm}{dt} = D 4\pi R^2 \left(\frac{\partial C}{\partial r}\right)_{r=R}, \tag{49}$$

where D is the diffusion coefficient of gas in the liquid and $(\partial C/\partial r)_{r=R}$ is the concentration gradient of gas dissolved in the fluid at the bubble surface. Clearly the rate of mass flow depends on the surface area of the bubble. The concentration of gas in the fluid obeys the diffusion equation

$$\frac{\partial C}{\partial t} = D \nabla^2 C, \tag{50}$$

where the convective term has been neglected; the motion of the fluid caused by the bubble shrinking is assumed small. Evaluating the dissolving time of a linearly oscillating bubble in an undersaturated solution reduces to the problem of a static bubble with a gas pressure P_0 in such a solution plus a correction that is second order in the small oscillation amplitude. For the static bubble, we solve the diffusion equation (50) subject to the conditions $C(R,t) = C_0$ and $C(r,0) = C_i = C_\infty$, where C_0 is the saturated concentration of gas in the fluid and C_i is the initial (undersaturated) concentration. Neglecting the velocity of the shrinking bubble wall, the solution is[17]

$$\left(\frac{\partial C}{\partial r}\right)_R = (C_i - C_0)\left[\frac{1}{R} + \frac{1}{(\pi D t)^{1/2}}\right]. \tag{51}$$

For long times the first term in braces dominates. Equating the mass flow given in (49) to the change in volume of the bubble gives the time for a bubble to dissolve from a radius R_0 to zero:

$$t_D = \frac{1}{2}\frac{\rho_0 R_0^2}{D(C_0 - C_i)}, \tag{52}$$

which for a ten micron air bubble in very undersaturated water is about one second, using $D = 2\times 10^{-9}$ m^2/sec and $C_0 = 0.02$ kg/m^3. This rather long time scale explains how the SL bubble can be stable at ambient size for a large fraction of the acoustic cycle (Fig. 1).

In a saturated solution (i.e., $C_0 = C_i$), the above argument is no longer valid. In this case each cycle of the bubble's oscillation, even in the limit of small-amplitude motion, leads to a net growth of the bubble, referred to as rectified diffusion.[18] This instability is not relevant to the range of parameters characterizing stable SL. Instead, for these parameters mass diffusion permits a steady-state solution, where the bubble's nonlinear motion counteracts its tendency to dissolve in the degassed solution. For these higher drive amplitudes the bubble's oscillation no longer scales with R_0, but instead the bubble can expand to a maximum determined by the drive, as in (31). To determine the dependence of R_0 drive parameters we consider the complete diffusion equation in the liquid,

$$\frac{\partial C}{\partial t}+\frac{\dot{R}R^2}{r^2}\frac{\partial C}{\partial r}=D\nabla^2 C, \tag{53}$$

where the velocity of the fluid $v=\dot{R}R^2/r^2$ in the incompressible limit of (18). Following the analysis of Eller and Flynn,[18] we eliminate the convective term by changing variables to the moving reference frame,

$$h=\tfrac{1}{3}(r^3-R^3),$$

where $R(t)$ is the radius of the bubble as it obeys the R–P equation. If we define a new time variable,

$$\tau(t)=\int^t R^4(t')dt', \tag{54}$$

the diffusion equation for $C(h,\tau)$ becomes

$$\frac{\partial C}{\partial \tau}-D\frac{\partial}{\partial h}\left[\left(1+\frac{3h}{R^3(\tau)}\right)^{4/3}\frac{\partial C}{\partial h}\right]=0. \tag{55}$$

The boundary condition for C at the bubble surface is determined by a generalization of Henry's law:

$$C(R)=C_0\frac{P_g(R)}{P_0}=\frac{C_0R_0^3}{R^3}, \tag{56}$$

viz. the concentration of gas in the fluid at the fluid/gas interface is proportional to the pressure of gas inside the bubble.[19] Here we have assumed that the equation of state of the bubble contents is isothermal rather than adiabatic (cf. Sec. VI). In the new coordinates the boundary conditions are

$$C(0,\tau)=\frac{C_0R_0^3}{R^3(\tau)} \tag{57}$$

and

$$C(\infty,\tau)=C_\infty, \tag{58}$$

i.e., that the ambient gas concentration in the fluid is constant. In the steady state the diffusion equation (55) can be simplified since $R(t)$, and therefore $R(\tau)$, are periodic functions. A spherical boundary whose concentration varies with a frequency ω will affect the fluid around it only in a region determined by the diffusive penetration depth,

$$\delta_D=\sqrt{\frac{2D}{\omega}}.$$

For the steady-state bubble motion the smallest frequency is that of the acoustic drive; the corresponding penetration depth is ~ 0.1 μm. Neglecting terms of $O(\delta_D/R_m)$ and higher we can keep only the leading term of the factor multiplying $\partial C/\partial h$ in (55) and thus obtain a one-dimensional diffusion equation,

$$\frac{\partial C}{\partial \tau}-D\frac{\partial^2 C}{\partial h^2}=0. \tag{59}$$

The formal solution to (59) subject to (57) and (58) can be written as a Fourier sum,

$$C(h,\tau)-c_\infty=A_0+\sum_{n=1}^{\infty}[(A_n\cos(k_nh-\Omega_n\tau)+B_n\sin(k_nh-\Omega_n\tau)]e^{-k_nh}, \tag{60}$$

where

$$\Omega_n=\frac{2\pi n}{\tau(T_a)} \quad \text{and} \quad k_n=\sqrt{\frac{\Omega_n}{2D}},$$

and $\tau(T_a)$ is the period of the dilated time variable τ. The boundary condition (57) specifies the Fourier coefficients. The mass flow is given by (49), which, in terms of h and τ, is

$$\Delta M(\tau)=\int_0^\tau 4\pi D\left(\frac{\partial C}{\partial h}\right)_{h=0}d\tau. \tag{61}$$

The preceding analysis requires not only that the net mass flow per cycle be zero to establish a steady state, but also that the mass in- or outflow at any point within a cycle be small compared to the total mass in the bubble, i.e.,

$$\frac{\Delta M(\tau)}{\frac{4}{3}\pi\rho_0R_0^3}\ll 1. \tag{62}$$

If this condition is not met, the equations governing diffusion and bubble motion cannot be separated; the R–P equation must be solved for a bubble with a non-mass-conserving equation of state, which is self-consistently given by mass diffusion coupled to the bubble dynamics.

The simplification of (55) to yield (59) used a penetration depth argument valid only for periodic solutions of $C(h,\tau)$. By contrast the constant term A_0 in the formal solution of (60) implies a dc flow to infinity that is not included in this approximation. The self-consistency of a steady-state solution thus requires that A_0 be identically zero, i.e.,

$$C_\infty=\frac{1}{\tau(T_a)}\int_0^{T_a}\frac{C_0R_0^3}{R^3(\tau')}d\tau'. \tag{63}$$

For a given set of drive parameters and R_0, (63) specifies the necessary concentration of gas in the fluid. For a physical system described by P_a, ω_a, and the new experimental parameter C_∞, (63) determines the steady-state value of R_0.

The motion of a bubble driven at an amplitude higher than those required to excite simple linear oscillations, yet not high enough to generate the catastrophic collapse and radiation of energy associated with SL, is shown in Fig. 6. This experimentally observed subsonic "bouncing" motion is completely described by the R–P equation. Using the drive parameters and value of R_0, which agree with the data to solve for $\tau(t)$ and $R(\tau)$, (63) yields value for C_∞. For bouncing motion this value is in accord with the gas concentration measured by means of dissolved oxygen ampules ($C_\infty\approx 0.05C_0$). As the solution becomes gassy, the value of C_∞ obtained by application of (63) to light-scattering measurements approaches the saturated value C_0.

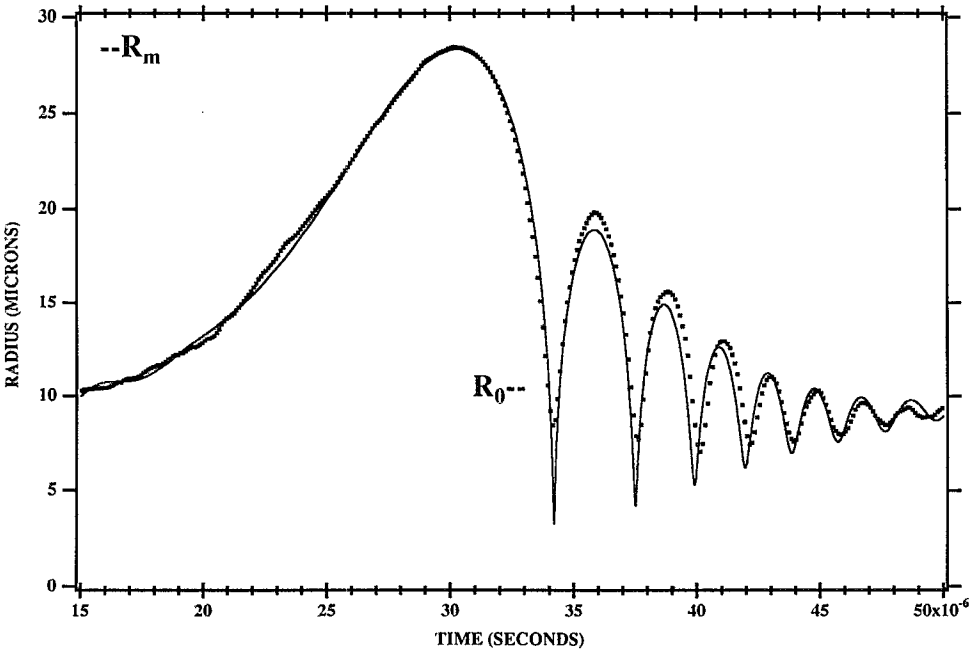

FIG. 6. The radius as a function of time for a bubble driven with an amplitude below the SL threshold. The dots are experimental data from light scattering from a non-light-emitting bubble. The solid line is a solution to (9) for $P_a=1.075$ atm, $\omega_a=2\pi$ (26.5 kHz), $R_0=10.5$ μm, $\eta=0.007$ kg/m sec, and $\sigma=0.03$ kg/sec^2.

However the same procedure applied to bubble motion in the SL regime, in the same degassed solution as the bouncing motion, yields a value for C_∞ that is about ten times too small. Such a result is also obtained analytically in the form of a scaling law for R_0. For SL bubble motion where $R_m \approx 10R_0$ the time variable τ is heavily weighted by the time spent near the maximum radius. Assuming that only the maximum contributes to τ in (63) yields the scaling law for R_0:

$$R_0=\xi\left(\frac{C_\infty}{C_0}\right)^{1/3} R_m, \tag{64}$$

where ξ is a scaling factor close to unity. A comparison of (64) to the definition of R_∞ (48) shows that the scaling law for R_0 implies $R_m \approx R_\infty$. In the highly nonlinear bubble motion characterizing SL, diffusion is determined exclusively by R_m; the steady state requires that R_∞ be sufficiently large that both mass in- and outflows are established at the large radii. The resultant C_∞ is thus correspondingly low.

Mass diffusion coupled to bubble motion seems to describe quite accurately the steady-state bouncing motion of a bubble driven below the SL threshold. In particular, the analysis introduces the ambient concentration of gas in the fluid as a relevant experimental parameter in determining the bubble dynamics and indicates how the solubility characteristics of the gas and fluid could affect the bubble motion. The incompatible results obtained from applying similar arguments to the bubble dynamics characterizing stable SL implies the insufficiency of the simplest model of mass diffusion to describe the SL bubble motion. There are numerous possible effects not included in our analysis. The linear relation between concentration and pressure implied by Henry's law is surely violated at the high pressures characterizing R_c. In particular, one could wonder if accompanying the sudden collapse is a burst of mass into the fluid that is not described by the simple diffusion equation. Our development has assumed a gaseous bubble; perhaps the transition from bouncing motion to SL marks the change in nature of the bubble contents from gas to vapor. Also, while the diffusion equation (55) has included the effect of a moving boundary, the formulation has neglected any far off-equilibrium phenomena such as mass convection cells in the fluid surrounding the bubble.

VI. HEAT DIFFUSION AND THE EQUATION OF STATE

The analysis thus far has assumed strictly adiabatic expansion and compression of the bubble contents, which clearly is an oversimplification of the bubble dynamics. In particular, the relatively slow velocities characteristic of the expansion phase should allow the bubble contents to exchange heat with the surrounding temperature bath.

The thermal penetration depth, $\delta_T=(2\kappa/\rho c_p\omega)^{1/2}$, where κ is the thermal conductivity of the medium and c_p is the specific heat at constant pressure, is a characteristic length scale for the diffusion of heat into the medium.[20] We use this to estimate the heat flux $q \propto \kappa(\partial T/\partial r)_{r=R}$ at the bubble surface. In the fluid

$$q \propto \frac{\kappa[T_0-T(R)]}{\delta_{Tl}}, \tag{65}$$

where T_0 is the ambient temperature of the fluid and $T(R)$ is the temperature at the bubble surface. In the gas,

$$q_g \propto \kappa_g \frac{[T(R)-T(0)]}{\delta_{Tg}}, \tag{66}$$

where $T(0)$ is the temperature at the center of the bubble. Equating heat fluxes at $r=R$ yields the comparison[21]

$$\frac{T_0-T(R)}{T(R)-T(0)}=\left(\frac{\kappa_g c_{pg}\rho_g}{\kappa c_p \rho}\right)^{1/2}. \tag{67}$$

Since the rhs of (67) is much less than unity for, say, air and water, the temperature variation in the fluid can be neglected. For purposes of analysis the fluid can be considered a perfect heat conductor; the boundary condition at $r=R$ may be taken as $T=T_0$.

To calculate the heat diffusing out at R_c we use the expression for the heat flow:

$$\Delta Q=\int dt\, R^2\left(\frac{\partial T}{\partial r}\right)_R \kappa\, 4\pi. \tag{68}$$

To estimate the temperature gradient we use the thermal penetration depth in the gas,

$$\delta_{Tg}=\left(\frac{2\kappa_g}{\rho_g c_{pg}}\frac{1}{\omega_c}\right)^{1/2}, \tag{69}$$

where κ_g, the thermal conductivity of air, varies with temperature as[21]

$$\kappa_g=(5.3\times 10^{-5}\ T+1.2\times 10^{-3})\text{J/m sec K}. \tag{70}$$

[This linear relation is valid in the range 200–3000 K. To obtain qualitative results we extrapolate it to the regime of dilute gases, where $\kappa_g \sim \sqrt{T}$, and hot, dense gases where $\kappa_g(T)$ is unknown.] Using ω_c and Δt_c defined by (40) and (55), the heat outflux at the minimum is

$$\Delta Q_{\text{out}}=\frac{4\pi^2 a^2 \kappa_g(R_c)(T_c-T_0)}{\delta_{Tg}(R_c)\omega_c}. \tag{71}$$

For typical parameters the ratio $\Delta Q_{\text{out}}/C_V$ of heat diffusing out to the net heat capacity of the bubble contents implies an equivalent temperature change of hundreds of degrees from the maximum temperature attained in the purely adiabatic compression of thousands of degrees. Thus the bubble collapse is well described by the adiabatic equation of state.

A similar calculation of ΔQ_{in} during the expansion phase yields an equivalent temperature change of hundreds of degrees from the adiabatic value, which at R_m is typically less than 100 K. Thus the calculation leads to a contradiction as regards the adiabatic expansion. In its stead we seek a solution to the fluid equations that allows for heat to flow from the fluid to the gas during the slow expansion. The relevant solution (cf. Appendix A) yields a heat flow, in accordance with Boyle's law for the isothermal expansion of an ideal gas, viz., the heat to flow in when the bubble grows from $R=R_0$ to $R=R_m$ is

$$\Delta Q_{\text{in}}=4\pi P_0 R_0^3 \ln\frac{R_m}{R_0}. \tag{72}$$

The subsequent slow compression of the gas from R_m to R_0 is accompanied by the equivalent outflux of heat; thus the temperature of the bubble deviates but slightly from the constant value.

In a cycle of its motion the net energy change of the bubble should be zero to define a steady-state motion. Thus the heat to flow out of the gas during the compression should be balanced by an equivalent irreversible heat flow into the bubble during the rest of the cycle. Indeed, this criterion can be used to establish the deviation of the bubble's "average" temperature during the cycle from the ambient value. If the temperature in the bubble is $T_0-\Delta T$ during the cycle, there is an influx of heat,

$$\Delta Q_m=\frac{2\pi}{\omega_a}\kappa_g(T_0)4\pi R_0^2\,\Delta T\left(\frac{2\kappa_g(T_0)}{\rho_0 c_p}\frac{1}{\omega_a}\right)^{-1/2}, \tag{73}$$

where ω_a is the drive frequency. Equating (71) and (73) gives an estimate for ΔT. Alternatively, ΔT can be interpreted as a measure of the extent to which the bubble's expansion is not isothermal, i.e., the bubble cools down $O(\Delta T)$ degrees from the ambient value for large R.

The derivations of the scaling laws for the bubble motion (31), (33), and (42) assumed a strictly adiabatic equation of state for the gas inside the bubble. However, the arguments leading to the expressions for R_m (31) and φ_m (33) assumed that the expansion had already proceeded to such an extent that the gas pressure was negligible. While the energy equation (21) must be supplemented with the additional source/sink of energy of the heat flow,

$$Q=-\kappa\left(\frac{\partial T}{\partial r}\right)_R 4\pi R^2, \tag{74}$$

this energy flux is small compared to the sound absorption and emission, and the scaling relation for R_c and R_m remains accurate. Qualitatively, the potential well model still presents an insightful picture of the collapse. However, one can incorporate the change in equation of state of the gas into the potential well model by splitting the well into two separate pieces; isothermal motion for $R>R_0$ and adiabatic motion for $R<R_0$. The additional integration constant may be fixed by requiring continuity of $\dot{R}$ at R_0.

The expression for the heat outflux at the minimum (71) can be used to calculate the contribution to the quality factor of the thermal conductivity. Using the definition (46) for Q_{th}, the energy of the system is found by

$$E_{\text{th}}=C_V\frac{4\pi}{3}R_f^3 T_0, \tag{75}$$

where C_V is the heat capacity of the fluid. The relatively large heat capacity of water, say, ensures that Q_{th} makes a negligible contribution to Q_{tot} for the sonoluminescing system. Nevertheless, the characterization of the bubble motion as more adiabatic or more isothermal is crucial to the theoretical understanding of a phenomenon that depends so strongly on thermodynamic variables.

VII. CONCLUSIONS AND OUTLOOK

According to the hydrodynamic theory of cavitation, the nonlinear oscillations of a bubble can focus the diffuse energy of the driving sound field to a small region for a short time, generating conditions appropriate to the traditional mechanisms of SL light emission. In this paper we have derived scaling laws for the key parameters of this model. Our analysis of the R–P equation shows the dependence of both the general bubble motion (R_m, φ_m, and R_c) and the specific properties of the dramatic collapse associated with SL (P_c, T_c, and Δt_c) on the externally imposed constraints, which are the acoustic drive, fluid, and gas.

However, while the hydrodynamics provides a workable model for the initial stages of the focusing of the sound energy, the bubble motion in physical realizations of SL, as described by the R–P equation, violates the mathematical limits of the equation's applicability. As shown in Fig. 4, for typical drive parameters, the Mach number in the gas approaches unity as the bubble collapses. Forcing the theoretical parameters, Δt_c and T_c, to match the temporal and spectral data from experiment results in even more drastic deviations from the assumed equilibrium conditions within the bubble (cf. Appendix B).

These observations indicate the potentially important role of shock wave formation within the collapsing bubble, both as regards its effect on the bubble motion and as an intermediate step to the light emission.[22] In the basic hydrodynamic theory the energy concentration (as given by T_c and Δt_c) depends on the collapse to the van der Waals hard core and the associated adiabatic heating of the bubble contents. For an imploding shock wave the heating that accompanies its reflection from the origin is determined by transport phenomena. The self-similar solutions for the implosion of a shock front with zero thickness yield infinite collapse temperatures.[23] The dissipative processes that give the shock a nonzero width, δ, also limit the energy concentration. We estimate the peak temperature of the shock to scale as

$$\frac{T_c}{T_0}\simeq\left(\frac{R_0}{\delta}\right)^{(2/\alpha)(1-\alpha)}, \tag{76}$$

where α is the self-similarity exponent characterizing the motion of the shock front [$R_{\text{shock}}\sim A(-t)^{\alpha}$, $\alpha\sim 0.7$]. The relation (76) was derived under the assumption that the shock is launched as the bubble passes through its ambient radius during the collapse; the time scale associated with the maximum temperature is $\Delta t_c\sim\delta/c_0$, where c_0 is the speed of sound in the gas at STP. For a shock thickness corresponding to $\Delta t_c=50$ psec, the experimental bound on the duration of the light flashes, the collapse temperature is roughly 100 000 K.

Shock waves may prove the correct intermediate description of how energy is focused to heat up/excite the bubble contents. Nevertheless, the R–P equation and our analysis is a valid model of the expansion of the bubble to its maximum volume and the stages of the collapse preceding the shock wave emission. The discrepancies between experiment and theory beyond this range point the way to the physics missing from the simplest hydrodynamic description of SL. Likewise, the theoretically predicted dependences of SL on the drive parameters and the thermodynamic properties of the fluid and gas can guide the experiments, elucidating the characteristics and probing the limits of this energy-focusing phenomenon.

ACKNOWLEDGMENTS

We thank Paul H. Roberts, Robert Hiller, and Andrés Larraza for valuable discussions. We are especially grateful to P. H. Roberts for valuable insights regarding mass diffusion.

This research is supported by the U.S. Department of Energy, Office of Basic Energy Science, Division of Engineering and Geophysics; R.L. is supported in part by an AT&T Fellowship; B.P.B. is supported in part by the U.S. Department of Energy Division of Advanced Energy Projects.

APPENDIX A: ISOTHERMAL MOTION OF A BUBBLE

To calculate the heat flux associated with a nearly isothermal expansion and contraction of a bubble, we start from the equations of fluid mechanics for purely radial motion (in this derivation all subscripts "g" have been dropped):

the continuity equation,

$$\frac{\partial\rho}{\partial t}+v\frac{\partial\rho}{\partial r}+\rho\bar{\nabla}\cdot v=0; \tag{A1}$$

Euler's equation (neglecting viscosity),

$$\frac{\partial v}{\partial t}+v\cdot\frac{\partial v}{\partial r}=\frac{-1}{\rho}\frac{\partial P}{\partial r}; \tag{A2}$$

and the heat equation,

$$\frac{\partial T}{\partial t}+v\cdot\frac{\partial T}{\partial r}=\frac{1}{c_V}(\bar{\nabla}\cdot\bar{v})\frac{T}{\rho}\left(\frac{\partial P}{\partial\rho}\right)_T\left(\frac{\partial\rho}{\partial T}\right)_P+\frac{\kappa}{\rho c_V}\nabla^2T, \tag{A3}$$

where c_V is the specific heat at constant volume, $(\partial P/\partial\rho)_T$ is the isothermal speed of sound, and $(\partial\rho/\partial T)_p$ is the isobaric expansion coefficient.

During the expansion phase the contents of the bubble behave as an ideal gas, satisfying the corresponding equation: $P/\rho=(k_B/m)T$ where k_B is Boltzmann's constant and m is the mass of a gas molecule. Following Prosperetti,[21] we add T times (A1) to ρ times (A2), and use the ideal gas equation of state to yield an expression for the time dependence of the pressure,

$$\frac{d}{dt}P=-P\gamma(\bar{\nabla}\cdot v)+\frac{\kappa}{c_V}\nabla^2T. \tag{A4}$$

Since pressure equilibrates with the speed of sound rather than diffusing, the pressure can be taken as uniform within the bubble, i.e., $\nabla P=0$. Integrating (A4) subject to the boundary condition $v=\dot{R}$ at $r=R$ gives

$$v=\frac{\dot{R}}{R}r+\frac{\kappa}{c_V}\frac{1}{P\gamma}\left(\nabla T-(\nabla T)_R\frac{r}{R}\right). \tag{A5}$$

We now use v given above in (A3) to look for solutions to the diffusion equation.

The solution $T_a(r,t)$ appropriate to adiabatic bubble motion is characterized by the condition

$$\frac{\partial T_a}{\partial t} \gg \dot{R}\frac{\partial T_a}{\partial r}, \tag{A6}$$

i.e., that changes in temperature due to convection be negligible compared to uniform changes of state in the bubble. Subject to this condition the first and third terms of (A3) dominate and v, as given by (A5), is strictly linear in r. The solution for T_a,

$$T_a = T_0\left(\frac{R_0}{R}\right)^{3(\gamma-1)},$$

is the same as (11) for an ideal gas, where a is zero.

For isothermal motion we seek a solution of the form $T=T_0+\delta T(r,t)$, where $\delta T/T_0 \ll 1$. In this limit the bubble motion is assumed slow and thus the condition (A6) is replaced by

$$\frac{\partial \delta T}{\partial t} \sim \dot{R}\frac{\partial \delta T}{\partial r}. \tag{A7}$$

For this case both terms on the lhs of (A3) are second-order small and the dominant terms yield

$$\frac{3\dot{R}}{R} - \frac{3R^2}{P_0R_0^3}\frac{\kappa}{c_p}\left(\frac{\partial \delta T}{\partial r}\right)_R + \frac{R^3}{P_0R_0^3}\frac{\kappa}{c_p}\nabla^2\delta T = \frac{\kappa}{\rho_0 R_0^3}R^3\nabla^2\delta T. \tag{A8}$$

The solution to (A8) that satisfies the boundary condition that $\delta T(r=R,t)=0$ is

$$\delta T = \frac{(r^2-R^2)}{2}\frac{\dot{R}P_0R_0^3}{\kappa R^4}. \tag{A9}$$

The corresponding heat flux during the expansion is given by

$$Q = \kappa\int_{R_0}^{R_m} 4\pi R^2\left(\frac{\partial \delta T}{\partial r}\right)_R dt = P_0R_0^3 4\pi \ln\frac{R_m}{R_0}, \tag{A10}$$

which is the same result as follows from Boyle's law for an isothermal expansion from $R=R_0$ to $R=R_m$.

APPENDIX B: SHOCK WAVES AND THE BREAKDOWN OF THE HYDRODYNAMIC MODEL

The velocity potential inside the bubble (i.e., for $r<R$) satisfies the wave equation

$$\nabla^2\varphi_g - \frac{1}{c_g^2}\frac{\partial^2\varphi_g}{\partial t^2} = 0, \tag{B1}$$

provided that the Mach number $v_g/c_g \ll 1$, where v_g is the velocity of the molecules in the bubble. The appropriate spherically symmetric solution to the wave equation may be decomposed into Bessel functions,

$$\varphi_g = \int A(\omega) j_0\left(\frac{\omega r}{c_g}\right)e^{-i\omega t}\,d\omega, \tag{B2}$$

where $j_0(x)=\sin x/x$ and the coefficients $A(\omega)$ are determined by boundary conditions. The corresponding pressure inside the bubble is

$$P_g = -\rho_g\frac{\partial \varphi_g}{\partial t} = \rho_g\int A(\omega) i\omega j_0\left(\frac{\omega r}{c_g}\right)e^{-i\omega t}\,d\omega. \tag{B3}$$

If $\omega r/c_g \ll 1$ the Bessel function becomes a constant, independent of r. Subject to this condition the quantity $P_g(r,t)$ is simply $P_g(R)$ a uniform pressure inside the bubble.

For small-amplitude oscillations and the slow expansion of the bubble, the above inequality holds true. However, the short time scales governing the bubble's motion near its minimum may violate the condition $\omega r/c_g \ll 1$. Even when ωR is small, it is still possible for bulk nonlinear effects to cause nonuniformities in P_g. The point at which the approximation of a uniform pressure inside the bubble ceases to be valid may be described by means of a perturbation expansion of $\rho(r,t)$ and $v(r,t)$ inside the bubble in the presence of a moving boundary. Such an expansion gives the following dimensionless parameters, whose magnitude determines the breakdown of equilibrium:

$$\text{(a)}\quad \frac{\dot{R}^2}{c_g^2},$$

$$\text{(b)}\quad \frac{R\ddot{R}}{c_g^2}\left[\frac{1}{2}+3\frac{\rho_g}{c_g}\left(\frac{\partial c}{\partial \rho}\right)_g\right], \tag{B4}$$

$$\text{(c)}\quad \frac{R^2\dddot{R}}{\dot{R}c_g^2}.$$

When these parameters approach unity, the bubble interior can no longer be regarded as being in an equilibrium state. The Mach number (a) approaching unity constitutes the typical condition for the formation of a shock front: the individual fluid particles are moving as rapidly as a signal can propagate through the system. The term (b) of (B4) contains the factor $(\rho_g/c_g)(\partial c/\partial\rho)_g$, dependent on the equation of state of the gas. For a van der Waals gas, this factor is

$$\frac{\rho_g}{c_g}\left(\frac{\partial c}{\partial \rho}\right)_g = \left(\frac{\gamma-1}{2\rho_g}+\frac{\frac{4}{3}\pi a^3}{n}\right)\Big/\left(\frac{1}{\rho_g}-\frac{\frac{4}{3}\pi a^3}{n}\right), \tag{B5}$$

where $\frac{4}{3}\pi a^3$ is the hard core volume and n is the number of molecules in the bubble. This factor approaches unity as the volume of the bubble approaches $10\pi a^3/3$ and grows exceedingly rapidly as the bubble collapses on the hard core. The term (b) in (B4) describes the compression of the gas near the moving boundary. As the factor $R\ddot{R}/c_g^2$ becomes large the density profile in the bubble deviates ever more from a constant, becoming highly localized to the region nearest the bubble wall. Theoretically this allows for the formation of a shock front, even without high bubble wall velocities.

The term (c) of (B4) takes into account the sound radiated into the bubble by the moving wall. This effect becomes important when the frequency characterizing the wall's motion $\omega=(\ddot{R}/\dot{R})^{1/2}$ exceeds the fundamental fre-

quency characteristic of the sphere. At such frequencies the state of the bubble's motion depends crucially on its history; thus emission of sound waves and their subsequent reflections need to be accounted for.

From numerical estimates it is clear that SL probes the limits of the hydrodynamic theory. For parameters in agreement with experiment, this basic theoretical analysis suggests the formation of shock fronts within the collapsing bubble.

The quantities of interest for the breakdown of equilibrium follow from the equations of fluid mechanics as they describe the bubble's interior. Assuming it is isentropic the equations relating to purely radial motion assume the form (where the subscript "g" has been dropped)

$$\frac{\partial \rho}{\partial t}+\frac{\partial(\rho v)}{\partial r}+\frac{2\rho v}{r}=0 \quad \text{(continuity)} \tag{B6}$$

and

$$\rho\left(\frac{\partial v}{\partial t}+v\frac{\partial v}{\partial r}\right)=-\frac{\partial P}{\partial r} \quad \text{(Euler's equation)}, \tag{B7}$$

where P is the pressure in the bubble. These equations are solved for a moving boundary at $r=R(t)$.

We expand the density $\rho=\rho_0+\rho_1+\rho_2+\cdots$ and the velocity $v=v_1+v_2+\cdots$, where the subscript denotes the order of smallness of the term. The velocity of the boundary is assumed small relative to the speed of sound in the gas, so that the relevant functions and operators may be grouped in the following orders of smallness: $O(1):\rho_0,\partial/\partial x$; $O(\epsilon):\rho_1,v_1,\partial/\partial t$; $O(\epsilon^2):\rho_2,v_2$, etc. The pressure in the gas is expanded as a function of density,

$$P(\rho)=P(\rho_0)+c^2(\rho_0)\delta\rho+\left(\frac{\partial c^2}{\partial \rho}\right)_0\frac{(\delta\rho)^2}{2}+\cdots, \tag{B8}$$

where $\rho=\rho_0+\delta\rho$ and the speed of sound $c^2=(\partial P/\partial\rho)_0$.

At zeroth order, Euler's equation becomes

$$\frac{\partial}{\partial r}P(\rho_0)=0, \tag{B9}$$

i.e., ρ_0 is a function only of time, not of coordinate. The lowest-order continuity equation:

$$\frac{\partial \rho_0}{\partial t}+\frac{\partial}{\partial r}\rho_0 v_1+\frac{2\rho_0 v_1}{r}=0, \tag{B10}$$

implies that v_1 is linear in r. Applying the boundary condition $v(R)=\dot{R}$ yields $v_1=\dot{R}r/R$. From (B10) we solve for $\rho_0(t)=\rho_{eq}(R_0^3/R^3)$ where R_0 is the initial radius of the bubble and ρ_{eq} is the initial (uniform) density inside.

The next nonzero contribution to ρ is defined by the equation

$$\rho_0\left(\frac{\partial v_1}{\partial t}+\frac{\partial}{\partial r}\frac{v_1^2}{2}\right)=-c_0^2\frac{\partial \rho_2}{\partial r}, \tag{B11}$$

where $c_0^2=c^2(\rho_0)$ is a function of time. Solving for ρ_2 gives

$$\rho_2=\frac{-\rho_0 r^2}{c_0^2}\frac{\ddot{R}}{2}\frac{}{R}. \tag{B12}$$

Finally, the third-order continuity equation yields the third-order velocity

$$v_3=\frac{1}{5}\frac{(r^3-R^3)}{c_0^2}\left[\frac{1}{2}\frac{\ddot{R}}{R}+\left[\frac{1}{2}+3\left(\frac{\partial c}{\partial \rho}\right)_0\frac{\rho_0}{c_0}\right]\frac{\ddot{R}\dot{R}}{R^2}\right]. \tag{B13}$$

The perturbation expansion is valid only when the ratios of subsequent terms (e.g., ρ_2/ρ_0 and v_3/v_1) are much smaller than unity. Evaluating these ratios using the above expressions shows that the parameters relevant to breakdown of equilibrium are (b) and (c). At this order of approximation the bubble wall Mach number, $M=\dot{R}/c_g$, does not appear. In fact, for the given initial conditions, ρ_0 and v_1 constitute an exact solution to the nonlinear wave equation when $\dot{R}(t)$ is constant. However, higher-order terms introduce the dependence on the Mach number; in order for the ratio ρ_4/ρ_2 to be small, the Mach number needs to be much less than unity.

[1] B. Barber, R. Löfstedt, and S. Putterman, "Sonoluminescence," J. Acoust. Soc. Am. Suppl. 1, **89**, S1885 (1991).

[2] D. F. Gaitan, L. A. Crum, C. C. Church, and R. A. Roy, "Sonoluminescence and bubble dynamics for a single, stable cavitation bubble," J. Acoust. Soc. Am. **91**, 3166 (1992); D. F. Gaitan and L. A. Crum, "Sonoluminescence from single bubbles," J. Acoust. Soc. Am. Suppl. 1, **87**, S141 (1990).

[3] B. P. Barber and S. J. Putterman, "Observation of synchronous picosecond sonoluminescence," Nature **352**, 318 (1991); B. P. Barber, R. Hiller, K. Arisaka, H. Fetterman, and S. J. Putterman, "Resolving the picosecond characteristics of synchronous sonoluminescence," J. Acoust. Soc. Am. **91**, 3061 (1992); R. Hiller, S. J. Putterman, and B. P. Barber, "The spectrum of synchronous sonoluminescence," Phys. Rev. Lett. **69**, 1182 (1992).

[4] Lord Rayleigh, "On the pressure developed in a liquid on the collapse of a spherical cavity," Philos. Mag. **34**, 94 (1917); M. Plesset, "The dynamics of cavitation bubbles," J. Appl. Mech. **16**, 277 (1949); B. Noltingk and E. Neppiras, "Cavitation produced by ultrasonics," Proc. Phys. Soc. B **63**, 674 (1950); Radiation damping is included by J. Keller and M. Miksis, "Bubble oscillations of large amplitude," J. Acoust. Soc. Am. **68**, 628 (1980); A. Prosperetti, "Physics of acoustic cavitation," Rendiconti S.I.F. **XCIII**, 145 (1984).

[5] C. Church, "A comparison between "real" and "ideal" gas in theoretical cavitation dynamics," J. Acoust. Soc. Am. Suppl. 2. **89**, 1862 (1991); B. P. Barber and S. J. Putterman, in Ref. 3.

[6] B. Noltingk and E. Neppiras, in Ref. 4.

[7] V. Griffing, "The chemical effects of ultrasonics," J. Chem. Phys. **20**, 939 (1952); R. Verrall and C. Sehgal, "Sonoluminescence," Ultrasonics **25**, 29 (1987).

[8] B. P. Barber and S. J. Putterman, "Light scattering measurements of the repetitive supersonic implosion of a sonoluminescent bubble," Phys. Rev. Lett. **69**, 3839 (1992).

[9] A. J. Campillo, J. D. Eversole, and H. B. Lin, "Cavity quantum electrodynamic enhancement of stimulated emission in microdroplets," Phys. Rev. Lett. **67**, 437 (1991); H. Chew, "Radiation and lifetimes of atoms inside dielectric particles," Phys. Rev. A **38**, 4310 (1988); **37**, 4107 (1988); "Transition rates of atoms near spherical surfaces," J. Chem. Phys. **87**, 1355 (1987).

[10] L. D. Landau and E. M. Lifshitz, *Fluid Mechanics*, 2nd ed. (Pergamon, New York, 1987), Sec. 64.

[11] R, Löfstedt and S. Putterman, "Theory of long-wavelength acoustic radiation pressure," J. Acoust. Soc. Am. **90**, 2027 (1991).

[12] B. Noltingk and E. Neppiras, in Ref. 4, has the incompressible form.

[13] P. Smereka, B. Birnir, and S. Banerjee, "Regular and chaotic bubble oscillations in periodically driven pressure fields," Phys. Fluids **30**, 3343 (1987).

[14] K. Yosioka and Y. Kawasima, "Acoustic radiation pressure on a compressible sphere," Acustica **5**, 167 (1955).

[15] R. Apfel, "Possibility of microcavitation from diagnostic ultrasound," IEEE-UFFC **33**, 139 (1986).

[16]J. B. Marion, *Classical Dynamics of Particles and Systems* (Academic, New York, 1970).
[17]P. S. Epstein and M. S. Plesset, "On the stability of gas bubbles in liquid–gas solutions," J. Chem. Phys. **18**, 1505 (1950).
[18]D.-Y. Hsieh and M. S. Plesset, "Theory of rectified diffusion of mass into gas bubbles," J. Acoust. Soc. Am. **33**, 206 (1961); A. Eller and H. G. Flynn, "Rectified diffusion during nonlinear pulsations of cavitation bubbles," J. Acoust. Soc. Am., **37**, 493 (1965).
[19]E. Fermi, *Thermodynamics* (Dover, New York, 1936), Sec. 130.
[20]L. D. Landau and E. M. Lifshitz, in Ref. 10, Sec. 52.
[21]A. Prosperetti, L. Crum, and K. Commander, "Nonlinear bubble dynamics," J. Acoust. Soc. Am. **83**, 502 (1988); E. Neppiras, "Acoustic cavitation," Phys. Rep. **61**, 159 (1980).
[22]L. J. Trilling, "The collapse and rebound of a gas bubble," J. Appl. Phys. **23**, 14 (1952); P. Jarman, "Sonoluminescence: A discussion," J. Acoust. Soc. Am. **32**, 1459 (1960); F. I. Bykovtsev and G. S. Rozarenov, "Pulsation of a spherical bubble in an incompressible fluid," Fluid Dyn. Sov. Res. **10**, 322 (1975); R. Löfstedt, B. P. Barber, R. Hiller, and S. J. Putterman, "Limitations of the hydrodynamic theory of cavitation-induced sonoluminescence," J. Acoust. Soc. Am. Suppl. 1, **91**, S2331 (1992); W. C. Moss, D. B. Clarke, R. A. Day, and J. W. White, "Bubble implosion and picosecond sonoluminescence," preprint.
[23]The solution of Guderley ["Starke Kugelige and Zylindrische Verdichtungsstösse in der Nähe des Kugelmittelpunktes bzw. der Zylinderachse," Luftfahrtforschung, **19**, 302 (1942)] is discussed in L. D. Landau and E. M. Lifshitz, in Ref. 10, Sec. 107.